



**HAL**  
open science

# Self-oscillating polymer membranes with chemically fueled pore size oscillation mediated by pH-responsive polymer

Johanne Pirkin-Benameur, Denis Bouyer, Damien Quemener

## ► To cite this version:

Johanne Pirkin-Benameur, Denis Bouyer, Damien Quemener. Self-oscillating polymer membranes with chemically fueled pore size oscillation mediated by pH-responsive polymer. *Journal of Membrane Science*, 2022, 658, pp.120742. 10.1016/J.MEMSCI.2022.120742 . hal-03736421

**HAL Id: hal-03736421**

**<https://hal.umontpellier.fr/hal-03736421v1>**

Submitted on 4 Oct 2023

**HAL** is a multi-disciplinary open access archive for the deposit and dissemination of scientific research documents, whether they are published or not. The documents may come from teaching and research institutions in France or abroad, or from public or private research centers.

L'archive ouverte pluridisciplinaire **HAL**, est destinée au dépôt et à la diffusion de documents scientifiques de niveau recherche, publiés ou non, émanant des établissements d'enseignement et de recherche français ou étrangers, des laboratoires publics ou privés.

# 1 Self-oscillating polymer membranes with chemically fueled 2 pore size oscillation mediated by pH-responsive polymer

3  
4 Johanne Pirkin-Benameur, Denis Bouyer, Damien Quemener\*

5 Institut Européen des Membranes, IEM-UMR 5635, Univ Montpellier, ENSCM, CNRS,34090 Montpellier,  
6 France.

7 \*Corresponding author

8 Email address: [damien.quemener@umontpellier.fr](mailto:damien.quemener@umontpellier.fr) (D. Quémener)

## 9 10 Abstract

11  
12 Soft-matter materials research has considerably evolved in the last decades, mainly by promoting responsive  
13 polymer systems. Up to now, the dynamic behavior in materials was always reached by the action of an outside  
14 trigger (pH, light, etc.). This constraint has been relieved in a new class of materials that experienced self-  
15 oscillation. In this work, the self-regulating pH cycles caused by a chemical oscillator will induce autonomous  
16 pH-sensible polymer chain movements at the membrane interface, causing continuous pore-size oscillation  
17 cycles and thus a self-oscillating flux. This work involved the functionalisation of polyethersulfone commercial  
18 membranes to achieve pore size oscillations. The pH-sensitive polymer, poly(methacrylic acid) (PMAA), was  
19 obtained by deprotection of poly(tert-butyl methacrylate) (PtBuMA) synthesized by RAFT polymerization. To  
20 adapt this functionalisation to all types of commercial membranes, a thin layer of polydopamine (PDA) was  
21 deposited on the top of the membrane, which then allows a Michael-thiol-ene reaction between PDA and thiol-  
22 functionalised PMAA, obtained from prior aminolysis of PtBuMA. The functionalisation steps were  
23 characterized by XPS, SEM, water contact angle, and permeability measurements. Membranes were then placed  
24 in a filtration system containing a chemical pH oscillator to control the PMAA chain conformation through the  
25 pH cycle. Water permeation analysis showed a dependence between permeability and PMAA conformation,  
26 leading to the conclusion that there is indeed a continuous oscillation in membrane pore size.

## 27 Keywords

28  
29 Self-oscillating membrane; pH oscillator; stimuli-responsive membrane; polydopamine; pH-sensitive polymer

30  
31

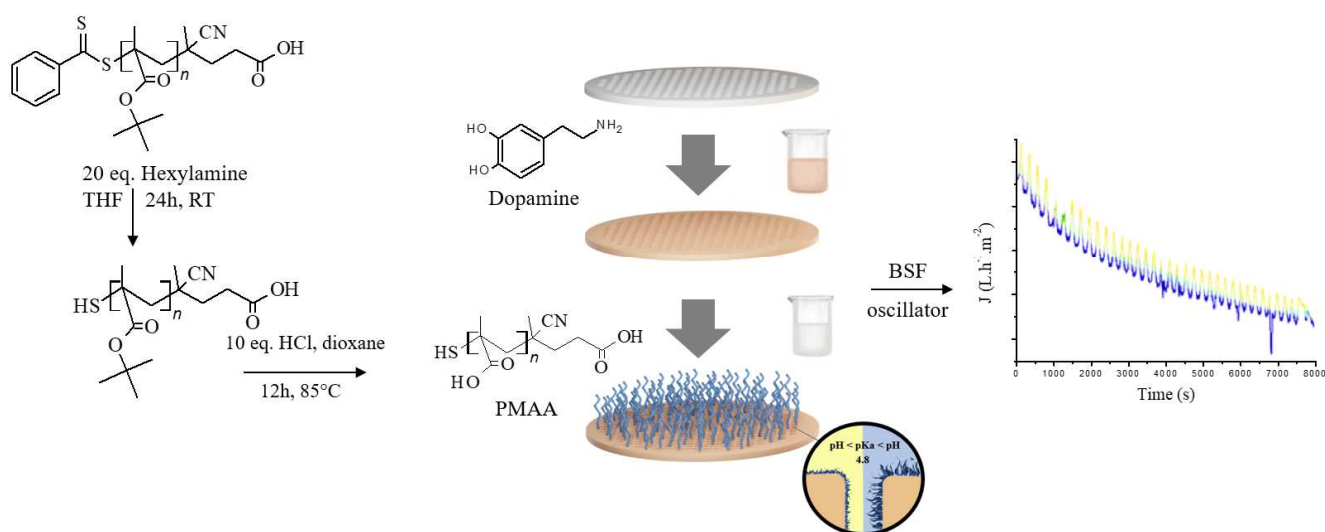
## 32 1. Introduction

33 Our century is filled with many issues, such as chemical pollution [1], which is partly caused by the lack of  
34 responsiveness of current materials. This problem and resource shortages are forcing us to develop materials  
35 with an improved lifespan, notably through new functionalities. Nature creates materials that meet this challenge,  
36 because of their advanced compositions and functions. Thus, one of the major challenges in the materials field is  
37 to reach the autonomy level of natural materials. Nowadays materials explored to mimic the nature include  
38 stimuli-sensitive systems [2]. Several stimuli have been studied to that purpose such as temperature [3], pH [4],  
39 mechanical strength [5], biological triggers [6], and electromagnetic fields [7] for applications such as  
40 chromatography [8], surface functionalisation [9], and sensor [10]. pH being one of the most common variables  
41 for biological reactions[11,12], pH sensitive polymers have found various applications, especially in biomedical  
42 field [13]. pH-sensitive membranes have also been developed due to the potential brought by this trigger such as  
43 stimuli-responsive permeation [14], pore size change [15,16], nanoparticle fractionation[17], or antifouling  
44 properties [18]. The pH responsiveness was introduced either during the membrane formation [19–21] or via a  
45 post functionalisation [17,18,22–24]. However, the limitation of these membranes, and materials in general, is  
46 that they must be “manually” activated and deactivated by triggering the corresponding stimulus [25]. Materials  
47 that cross this boundary gains autonomy, whether it is by allowing self-protection [26], self-reporting [27], self-  
48 healing [28], regenerating [29], or controlled degradation ability [30].

49 A standalone promising feature in this category that has recently been reported is self-oscillation. It involves  
50 coupling a sensitive material with a chemical oscillator. A chemical oscillator is a network of chemical reactions  
51 in which the concentration of the products changes on a cyclic basis until the source of energy is exhausted.  
52 When coupled to a material, continuous periodic variation of macroscopic properties such as its volume or its  
53 hydrophobic-hydrophilic balance is observed. Since the first self-oscillating materials developed by Yoshida  
54 [31], many works have been carried out with the Belousov-Zhabotinsky (BZ) oscillator, such as self-walking gel  
55 [32], self-oscillating gel for mass transports [33], soft actuators of organized self-oscillating microgels [34] or  
56 self-oscillating chemoelectrical interface of solution-gated ion-sensitive field-effect transistor [35]. This concept  
57 doesn't allow only to create new materials, but also to discover new possibilities with well-known polymer  
58 properties like lower critical solution temperature autonomously modulated by photo-regulation [36]. Despite  
59 the accomplishments already reached, the self-oscillating field still has a high potential, with recent progress  
60 achieved to precisely control the mechanical oscillation[37,38], or simply by getting even closer to what nature  
61 is capable of. Indeed, in all the biological phenomena, the cellular membrane is a wonderful model because of  
62 the astonishing possibilities of action, from formation to self-destruction, only triggered by the membrane  
63 environment. Being able to reach this complexity level would resolve most of the issues in the membrane field.  
64 To achieve this objective, our group recently introduced the concept of self-oscillating filtration membranes  
65 [39]. From an alumina membrane functionalized by a pH-sensitive polymer, pH oscillations in the filtration cell  
66 made it possible to obtain transmembrane flux oscillations. The principle relies on a change in conformation of a  
67 polymer chain as a function of the pH which leads to cycles of opening and closing of the membrane pores.

68 Here a new strategy is proposed to explore a universal method of introducing self-oscillation functionality to  
69 all types of membranes, in particular polymer membranes. The overall strategy is depicted in Figure 1. The

70 principle is based on the synchronization between a pH oscillator, here Bromate-Sulfite-Ferrocyanide (BSF) and  
 71 a membrane made pH-sensitive. To obtain this membrane, poly(methacrylic acid) (PMAA) was chosen as a pH-  
 72 sensitive polymer thanks to its pKa at 4.8 [39]. PMAA is synthesized by Reversible Addition-Fragmentation  
 73 Chain Transfer (RAFT) polymerization of tert-butyl methacrylate (tBuMA), followed by hydrolysis of the  
 74 resulting PtBuMA. After aminolysis of the RAFT end group, the PMAA chains are terminated by a thiol  
 75 function which will be used subsequently for their grafting onto the membrane. To make this grafting possible  
 76 regardless of the type of membrane, a thin layer of polydopamine is first deposited. A Michael thiol-ene reaction  
 77 between PMAA and polydopamine then allows membrane functionalisation. In the presence of the pH oscillator,  
 78 cycles of change in the conformation of the PMAA chains allow for a cyclic change of the pore size and  
 79 therefore of the transmembrane flux. In this work, the influence of the polydopamine deposition time and the  
 80 PMAA molecular weight on the oscillation properties is particularly studied.



81

82 Figure 1 - General strategy carried out to produce self-oscillating polymer membranes

## 83 2. Experimental Part

### 84 2.1 Materials

85 Tert-butyl methacrylate 98%, containing 200 ppm monomethyl ether hydroquinone as inhibitor (Sigma) was  
 86 filtered through an inhibitor removing resin for 15 minutes before use. Azobisisobutyronitrile (Fluka) was used  
 87 after two recrystallizations in methanol. 4-cyano-4-(phenylcarbonothioylthio)pentanoic acid (Sigma), 1-  
 88 Hexylamine (Fluka, 99%), chlorohydric acid 37% in weight, (trimethylsilyl)diazomethane solution 2.0 M in  
 89 diethyl ether (Sigma) dopamine hydrochloride (Sigma), tris glycine buffer solution 10x concentrate (Sigma),  
 90 potassium bromate (Sigma), bromocresol green, dye content 95% (Sigma), potassium hexacyanoferrate(II)  
 91 trihydrate (Sigma), sodium sulfite (Sigma), sulfuric acid 99.9% (Sigma), bovine serum albumine (Sigma),  
 92 dextran from Leuconostoc with Mn= 6000 g.mol<sup>-1</sup>, Mn= 70000 g.mol<sup>-1</sup>, Mn= 100000 g.mol<sup>-1</sup>, Mn= 200000  
 93 g.mol<sup>-1</sup>, Mn= 500000 g.mol<sup>-1</sup>, Mn= 2 000000 g.mol<sup>-1</sup> (Sigma), were used as received. Commercial  
 94 polyethersulfone membranes with MWCO = 100 kDa, 63.5 mm diameter (Millipore®, PBHK06210) were  
 95 washed 1 h by immersion in MilliQ water with water being changed three times before use.

96

97 2.2. Synthesis and Membrane Functionalisation

98

99 2.2.1. RAFT Synthesis of poly(tert butyl methacrylate)

100

101 Tert-butyl methacrylate (tBuMA) is placed in a flask with DMF at [tBuMA]= 0.5g.mL<sup>-1</sup>, and the number of  
102 moles of AIBN and CTA corresponding to the target molar mass. As an example, the target ratio for M<sub>n</sub>PMAA of  
103 20000 g.mol<sup>-1</sup> is  $\frac{n_{CTA}}{n_{AIBN}} = 5$  and  $\frac{n_{monomer}}{n_{CTA}} = 141$ . The solution is then degassed with nitrogen in an ice bath for 30  
104 minutes. The reaction was carried out for 24 h at 70 °C. The polymer is then precipitated twice in a cold  
105 methanol/water mixture 4:1(v:v) and dried at room temperature under vacuum for 24h.

106

107 2.2.2 Aminolysis of poly(tert-butyl methacrylate)

108

109 The aminolysis procedure reported by Whittaker and al. [40] was adapted as follows: in a flask, PtBuMa is  
110 dissolved at a concentration of 6.5 ml/g in THF and cooled in an ice bath. A large excess of hexylamine  
111 ( $\frac{n_{hexylamine}}{n_{polymer}} = 20$ ) is cooled in an ice bath. The two solutions are placed in two separate flasks, before being  
112 degassed with nitrogen for 30 minutes in an ice bath. The hexylamine solution is added to the polymer solution  
113 by syringe under nitrogen flow. The reaction was carried out at room temperature for 20 hours. The polymer is  
114 precipitated in a methanol/water mixture 4:1 (v:v) and dried at room temperature under vacuum for 24h.

115

116 2.2.3 Deprotection of PtBuMA-SH

117

118 The protocol reported by Cazares-Cortes et al. [41] was adapted as follows: aminolyzed PtBuMa is  
119 dissolved in dioxane at a concentration [PtBuMA-SH] = 83 mg.mL<sup>-1</sup>. Under stirring, an excess of HCl ( $\frac{n_{HCl}}{n_{polymer}} = 10$ )  
120 is added dropwise, before allowing the reaction to reflux for 16 hours at 85°C. Approximately one third of  
121 the solvent was then evaporated on a rotary evaporator before precipitating the polymer in cooled diethyl ether.

122

123 2.2.4 Methylation of PMAA to poly(methyl methacrylate) (PMMA)

124

125 In order to check the molecular weight distribution of PMAA in organic medium and avoid its  
126 aggregation in water during its analysis, PMAA was methylated into poly(methyl methacrylate) (PMMA)  
127 before being characterized in Size Exclusion Chromatography in tetrahydrofuran. The protocol reported by  
128 Lacik et al. [42] was used and adapted as follows: PMAA is dissolved in a 1:1 (v:v) mixture of THF / water at a  
129 concentration of 5mg/mL and placed in a flask. Trimethylsilyldiazomethane is then added dropwise with stirring

130 until the yellow color is constant and no further off-gassing occurs. The flask is left to stir until the solution has  
131 completely decolorized (7h). The solution was then placed in a beaker in the fume hood and left in the open air  
132 until the solvent had evaporated completely.

133

## 134 2.2.5 PDA coating on commercial membranes

135

136 The protocol reported by Lee et al. [43] was adapted as follows: in a first step, three 24 mm diameter  
137 membranes are cut from the 64 mm commercial membrane, before being washed for 1 hour in Milli-Q water. A  
138 pH = 8.5 solution is prepared using a 10: 1 Milli-Q water/tris glycine buffer solution. Dopamine is added to  
139 obtain a concentration of 0.1 mg.mL<sup>-1</sup>. Membranes are then immersed 15 minutes directly to the dopamine  
140 solution under stirring (70 rpm). Once the reaction is complete, the membrane is washed directly with milli-Q  
141 water, then subjected to an ultrasound bath for 15 minutes, and stored in milli-Q water/ethanol 95:5 (v:v).

## 142 2.2.6 PMAA-SH grafting on PDA-coated membranes

143

144 A 10<sup>-5</sup> mol solution of PMAA is prepared in milli-Q water at pH = 8.5. The PDA-coated membrane is  
145 placed in the solution, and the reaction is carried out at 55°C for 2h. Once the reaction is complete, the  
146 membrane is rinsed with milli-Q water, subjected to an ultrasound bath for 15 minutes, and then stored in milli-  
147 Q water/ethanol 95 : 5 (v : v).

148

## 149 2.3 Polymer and membrane characterization

150

### 151 2.3.1 Polymer analysis

152

153 Proton Nuclear Magnetic Resonance (<sup>1</sup>H NMR) spectroscopy. The <sup>1</sup>H NMR analysis was performed  
154 with a Bruker Advance 400 MHz spectrometer. Samples were prepared in deuterated CDCl<sub>3</sub> for PtBuMA and  
155 MeOD for PMAA.

156 Size exclusion chromatography (SEC). Molecular weight distributions were assessed by SEC (Viscotek  
157 TDA 305, Malvern) using THF as eluent at a flow rate of 1.0 mL/min on a Polymer Laboratories PL-GPC 50  
158 instrument using two PL mixed C 5.0 μm columns at 35 °C and a refractive index detector. Calibration was done  
159 using Varian polystyrene narrow standards. Between 1 and 5 mg of polymer was dissolved in 1 ml of a solution  
160 of THF with 0.3% toluene (flow marker). The solution was filtered with a 0.22 μm filter before being introduced  
161 into the SEC.

162 Fourier Transform Infrared (FTIR) spectroscopy. FTIR analysis was performed with the FTIR 710  
163 Nicolet instrument (Thermo Electron Corporation). The analyses are performed in ATR mode with 64 scans and  
164 a resolution of 82 in transmission mode.

165 UV-Vis Spectroscopy. Polymer solutions before and after aminolysis were prepared at the same  
166 concentration. The analysis was performed in a glass cuvette with the UvLine connect series 940 (SECOMAM)  
167 from 200 to 800 nm in absorbance.

168

### 169 2.3.2 Membrane characterization

170

171 Water Contact angle (WCA). The WCA analysis was conducted with the ILMS GBX and Digidrop  
172 GBX software. The membrane is dried in an oven, before being glued to a support prior the analysis. WCA was  
173 measured with a drop volume of approximately 1.7  $\mu\text{L}$ . About 10 measurements are made before being averaged  
174 for each trial, and three trials are performed.

175 Scanning Electron Microscopy (SEM). SEM analyses were conducted using a Hitachi S-4500 (Tokyo,  
176 Japan) device operating at spatial resolution of 1.50 nm at 15 kV energy. The samples of 1cm x 0,5 cm were  
177 dried and coated with an ultrathin layer of electrically conducting platinum deposited by high-vacuum  
178 evaporation. Energy-dispersive X-ray spectroscopy analysis (EDX) was taken with Zeiss EVO HD15  
179 microscope coupled with an Oxford X-MaxNSDD EDX detector. Surface porosity has been obtained from  
180 binarized SEM images using Image J<sup>®</sup> software with  $\phi = \frac{\text{Area}_{\text{pores}}}{\text{Area}_{\text{total surface}}} \times 100$ .

181 Gravimetric analysis. Sample gain in weight after functionalization was estimated on samples dried for  
182 1 h in a vacuum oven at 50°C, before being weighed with a Precisa XT 220 A balance.

183 Porosity measurement. Membranes were previously weighed after drying for 2h in a vacuum oven at  
184 50°C, before being placed under ultrasound for 1 hour in a beaker of 1-butanol until no more bubbles escape  
185 from it. The membranes were then weighed directly after removal from the beaker and blotting excess of 1-  
186 butanol from the membrane surface. The equation for measuring the porosity (P) is as follows [44]:

$$187 \quad P(\%) = \frac{(W_2 - W_1)\rho_1}{\rho_1 W_2 + (\rho_2 - \rho_1)W_1}$$

188 with  $W_1$  = initial mass,  $W_2$  = mass after immersion in 1-butanol,  $\rho_1$  = polyethersulfone density (1.37 g.mol<sup>-1</sup>) and  
189  $\rho_2$  = 1-butanol density (0.8 g.mol<sup>-1</sup>)

190 Sieving curves. Dextran of different molecular weights were used to prepare aqueous solutions at a  
191 concentration of 1000 ppm. 10 ml was then poured into a dead end stirred filtration cell at 1 bar. The first 2mL  
192 of permeated water were discarded, and the next 4mL were taken as permeate solution. The last 4mL remaining  
193 in the filtration cell constituted the retentate solution. Membranes were washed 10 minutes in water under  
194 ultrasounds between each attempt. The solution signal was then analyzed by a Water 2414 refractive index  
195 detector.

196 Liquid-liquid porometry. It was conducted with PRM-2000-LL-R porometer from G.E.P.S. France.  
197 Prior to the measurement, same amount of MilliQ water and 1-butanol was “mixed” and let to separate by  
198 decantation in order to saturate the two phases. The aqueous and organic phases were then stored separately.

199 Before the porometry experiment, the membrane was completely soaked into the aqueous phase before being  
200 placed in a porometer cell. Increasing pressure from 0 to 6 bar was applied on the organic phase side of the  
201 membrane to progressively replace the aqueous phase.

202 Zeta potential measurement. The surface charge (zeta potential) of the membrane was estimated using  
203 SurPASS electrokinetic analyzer (Anton Paar, GmbH, Graz, Austria) based on the streaming potential method.  
204 Washed membrane samples were mounted in an adjustable gap cell and soaked in 1 mM KCl. The cell height  
205 was fixed at 100 mm. The electrolyte solution was circulated in the cell between two pieces of membrane. The  
206 zeta potential was calculated using the Helmholtz–Smoluchowski equation from the measured streaming current  
207 as a function of pH.

208 X-Ray photoelectron spectrometry (XPS). XPS was carried out with the ESCALAB 250 device from  
209 ThermoElectron. The excitation source was the monochromatic source, Al K $\alpha$  line (1486.6 eV). The surface  
210 analyzed has a diameter of 500  $\mu$ m. Photoelectron spectra were calibrated in binding energy with respect to the  
211 energy of the C-C component of carbon C1s at 284.8 eV.

212 pH analysis. The HI 5221 (Hanna) instrument was calibrated with pH 4, 7 and 9 buffer solutions.  
213 Measurements were then recorded every second.

214 Chemical resistance. Resistance of the membranes to the acidic and alkaline environments was  
215 estimated by comparing the initial water flux of the grafted membrane at 1 bar of pressure drop with the flux  
216 after an immersion of the membrane during 15 days at pH=3 for acidic condition, and pH=10 for alkaline  
217 condition.

218 Tensile test. Mechanical properties of the membrane were measured with a 5kN ProLine ZwickRoell  
219 universal testing machine and screw grips of 10kN. A 1x2cm sample membrane was cut and placed on the screw  
220 grip while still wet from the conservation solution. The measurement started with 2cm between the two screw  
221 grips.

222

### 223 2.3.3 Water permeation analysis and acquisition of oscillations

224

225 The 22 mm diameter membrane was placed into a homemade stainless steel 22 ml dead-end filtration  
226 cell. A 1L Amicon tank filled with MilliQ water was connected to the cell with adjustable pressure. Permeated  
227 water was measured using a balance connected to the S232 Data Logger software with a 0.599s time step  
228 acquisition. A conditioning step was applied to all membranes by applying a pressure drop of 4 bar during 30  
229 minutes before any permeability measurement.

230 For a water permeation under pH oscillations, aqueous feed solutions separated in two tanks entered  
231 premixed at the same flow rate into the dead end filtration cell (Figure SI28) (Tank 1: [KBrO<sub>3</sub>]<sub>0</sub> = 75 mM and  
232 [sodium bromocresol green]<sub>0</sub> = 2.15 · 10<sup>-3</sup> mM; Tank 2: [Na<sub>2</sub>SO<sub>3</sub>]<sub>0</sub> = 70 mM, [K<sub>4</sub>Fe(CN)<sub>6</sub>]<sub>0</sub> = 15 mM, [H<sub>2</sub>SO<sub>4</sub>]<sub>0</sub> =  
233 7.5 mM). BSF pH oscillator was set up in the filtration cell under pressure and the relative pH evolution was  
234 monitored by video acquisition of the solution color change thanks to a pH indicator (bromocresol) (Figure



235 SI28). The pH oscillator allows cyclic variations of the pH with wide and regular amplitude of oscillations  
 236 between 3.5 and 6.5 under the membrane filtration conditions (Figure SI24). The targeted  $k_0$  value, which  
 237 corresponds to the inverse of the residence time in the filtration cell, was  $1 \cdot 10^{-3} \text{ s}^{-1}$ .

### 238 2.3.4 Modeling of Bromide-Sulfite-Ferrocyanide (pH and ionic strength)

239

240 Bromate-sulfite-ferrocyanide (BSF) pH oscillator has been modeled as described in our previous work  
 241 [39]. The system of Ordinary Differential Equations (ODE) that described chemical reactions was numerically  
 242 solved using finite element software: COMSOL Multiphysics® 5.4. A variable time step was used to improve  
 243 the numerical resolution. The evolution of ionic strength (I) during pH oscillations was carried out by taking into  
 244 account the following ionic species:

245 Cations:  $\text{Na}^+$ ,  $\text{H}^+$ ,  $\text{K}^+$

246 Anions:  $\text{OH}^-$ ,  $\text{HSO}_4^-$ ,  $\text{SO}_4^{2-}$ ,  $\text{SO}_3^{2-}$ ,  $\text{HSO}_3^-$ ,  $\text{BrO}_3^-$ ,  $\text{Br}^-$ ,  $\text{HFe}(\text{CN})_6^{3-}$ ,  $\text{Fe}(\text{CN})_6^{4-}$

247 Ionic strength was calculated over time by the following equations:

$$248 \quad I = \frac{1}{2} \left( \sum_i C_i z_i^2 \right)$$

249  $C_i$ , being the molar concentration of ion  $i$  and  $z_i$  being the charge number of ion  $i$

$$250 \quad I = \frac{1}{2} ([\text{SO}_3^{2-}] \cdot (-2)^2 + [\text{HSO}_3^-] \cdot (-1)^2 + [\text{HSO}_4^-] \cdot (-1)^2 + [\text{SO}_4^{2-}] \cdot (-2)^2 + [\text{BrO}_3^-] \cdot (-1)^2$$

$$251 \quad + [\text{Br}^-] \cdot (-1)^2 + [\text{HFe}(\text{CN})_6^{3-}] \cdot (-3)^2 + [\text{Fe}(\text{CN})_6^{3-}] \cdot (-3)^2 + [\text{OH}^-] \cdot (-3)^2$$

$$252 \quad + [\text{Fe}(\text{CN})_6^{4-}] \cdot (-3)^2 + [\text{H}^+] \cdot (1)^2 + [\text{Na}^+] \cdot (1)^2 + [\text{K}^+] \cdot (1)^2$$

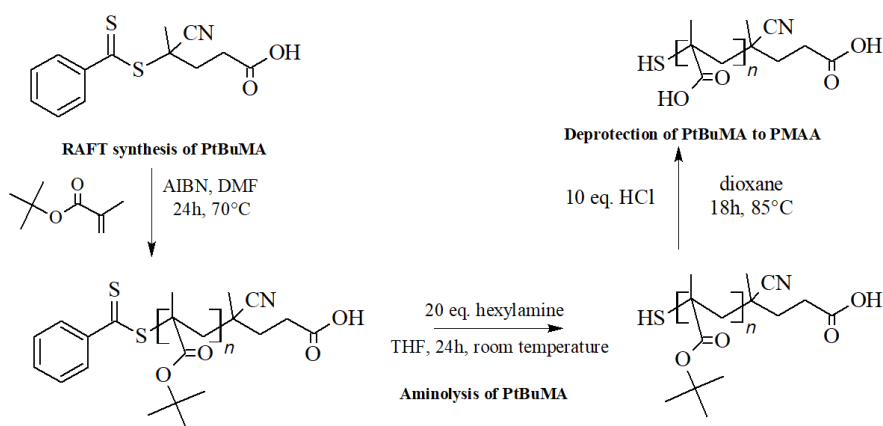
253

254

## 255 Results and Discussion

256

### 257 3.1 Polymer Synthesis



258

259 Scheme 1 – Overview of the thiol-functionalized polymethacrylic acid (PMAA) synthesis by RAFT  
 260 polymerization

### 261 3.1.1 RAFT synthesis of PtBuMA

262

263 In a first step, a thiolated pH sensitive PMAA was prepared by RAFT polymerization of tBuMA  
264 followed by its aminolysis and hydrolysis (Scheme 1). MAA was not polymerized directly as its corresponding  
265 PMAA polymer is not soluble in an organic solvent and hard to characterize in water due to its inclination to  
266 self-aggregate. The SEC curves of all PtBuMA polymers demonstrate distinct molecular weight distributions and  
267 low dispersity as expected from a controlled polymerization (Figure SI-1). PtBuMA was obtained with monomer  
268 conversions greater than 70% for all polymers (Table SI-1).

### 269 3.1.2 Aminolysis of PtBuMA

270

271 As previously explained, the grafting of PMAA onto the polymer membrane was carried out by a  
272 Michael thiol-ene reaction on a deposited polydopamine top layer. For that, an aminolysis of the RAFT end  
273 group is required to yield a thiol group at the end of the PtBuMa chain (Scheme 1).

274 The aminolysis was characterized by UV-visible spectroscopy following the absorbance peak at 300  
275 nm, related to the aromatic RAFT end group. A large decrease in the signal attests to the success of the reaction  
276 with a yield estimated up to 92% (Figure SI-2a, Table SI-1). The SEC curves before and after aminolysis (Figure  
277 SI-2b) demonstrate the integrity of the polymer after the reaction, although some slight chain-chain coupling was  
278 observed due to a thiol oxidation into disulphide.

### 279 3.1.3 Deprotection of PtBuMA from PMAA

280

281 The aminolyzed PtBuMA was then converted into PMAA by hydrolysis of the tert-butyl group. The  
282 completion of the reaction is shown by the disappearance of the tert-butyl signal in  $^1\text{H}$  NMR (Figure SI-6).

283 The FTIR spectra of the polymers were carried out after each step (Figure SI-3). The PtBuMA and  
284 aminolyzed PtBuMA spectra are nearly identical as expected, since the very low concentration of the RAFT end  
285 group does not enable any detection. Peak at  $2992\text{ cm}^{-1}$  is assigned to the C-H stretching of alkane, and  $1735\text{ cm}^{-1}$   
286 to the C=O stretching of ester group. After hydrolysis, FTIR spectrum of the resulting PMAA shows the  
287 appearance of a peak at  $3300\text{-}2500\text{ cm}^{-1}$  assigned to O-H stretching of the carboxylic acid group, as well as a  
288 peak at  $1715\text{ cm}^{-1}$  corresponding to the C=O stretching of the carboxylic acid group, in agreement with the  $^1\text{H}$   
289 NMR.

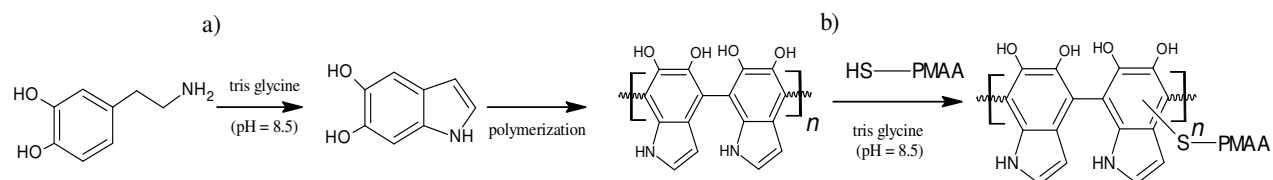
290 As previously reported [39], PMAA is difficult to characterize in aqueous SEC due to the presence of  
291 aggregates. To check the distribution of molecular weights after hydrolysis of the tert-butyl group, PMAA was  
292 methylated in poly(methyl methacrylate) (PMMA) and analyzed in THF SEC (Figure SI-4). A shift of the entire  
293 distribution toward lower molecular weights is observed, as expected, with a maintained low dispersity of 1.06.  
294 Note that the secondary pic corresponds to a double molecular weight, which is due to thiol-thiol coupling, as  
295 explained before.

296

297

### 298 3.2 Membrane functionalisation

299



301

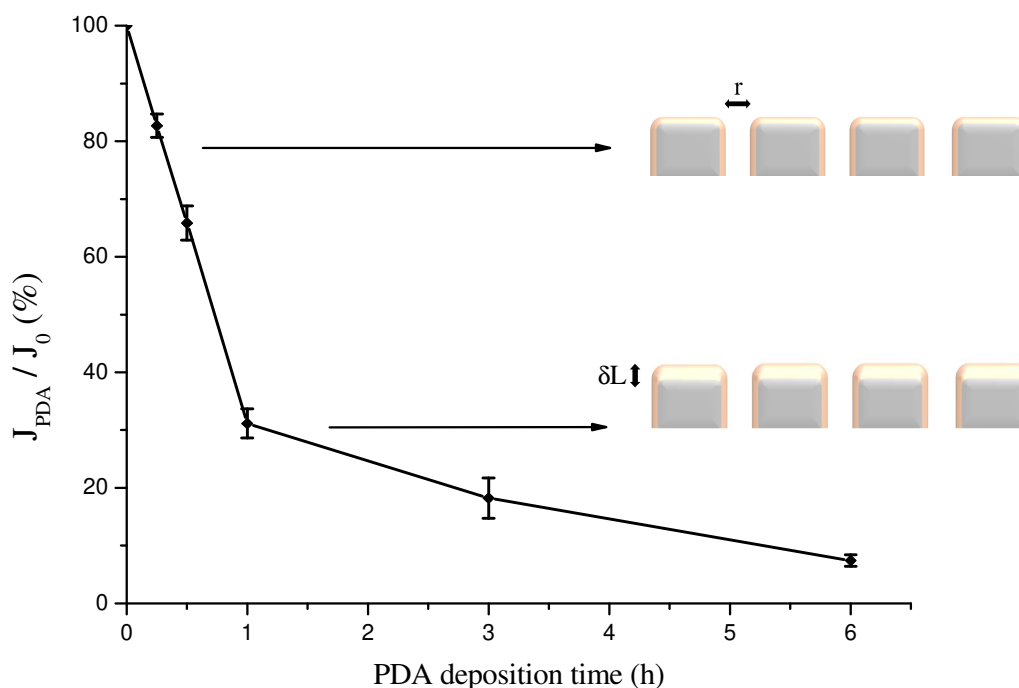


302

302 Figure 2 – a) Synthesis and coating of polydopamine onto polyethersulfone membrane followed by b) grafting of  
303 pH-sensitive PMAA chains through Michael thiol-ene reaction.

304 The functionalisation of a commercial polyethersulfone membrane (PES) by the pH sensitive PMAA  
305 was mediated through the deposition of a thin polydopamine (PDA) layer, as described in Figure 2. This  
306 technique, already reported in the literature [45], is very versatile and can be applied to all types of membranes  
307 without physicochemical constraints due to the ability of the PDA to stick anywhere. Polymer grafting was then  
308 performed simply by immersion of the PDA-coated membrane in a PMAA solution. This functionalisation  
309 process occurs in water under mild conditions, making any potential scale-up environmentally friendly.

310



311

312 Figure 3 – Evolution of the flux of the PES membrane after PDA deposition ( $J_{PDA}$ ) compared to the flux of the  
313 virgin membrane ( $J_0$ ).

314

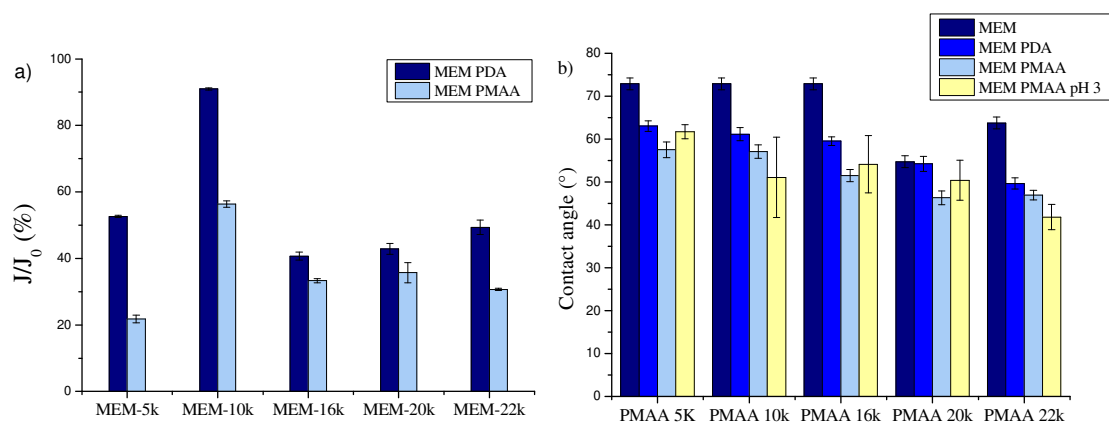
315 The permeance of the PDA coated membranes in Figure 3 shows a decrease correlated with the  
316 deposition time. In a first part, delimited by a PDA deposition time of less than 1 hour, a significant slope is  
317 observed while a clear break beyond this time marks a slower evolution. This distinction can illustrate two  
318 different flux reduction mechanisms. As the Poiseuille equation (1) shows, the flux can evolve by a change in the  
319 radius of the pores (to the power of 4), their number, and their length. Given the rapid evolution for short  
320 deposition times, we can hypothesize that a decrease in the pore diameter is the main factor involved in this first  
321 part. Then, the PDA coating increasing with time, the length of the pores, and the number of open pores certainly  
322 govern the evolution of the flux in the second part.

$$323 \quad J = \frac{N \cdot dP \cdot r^4}{8 \cdot \eta \cdot L} \quad (1)$$

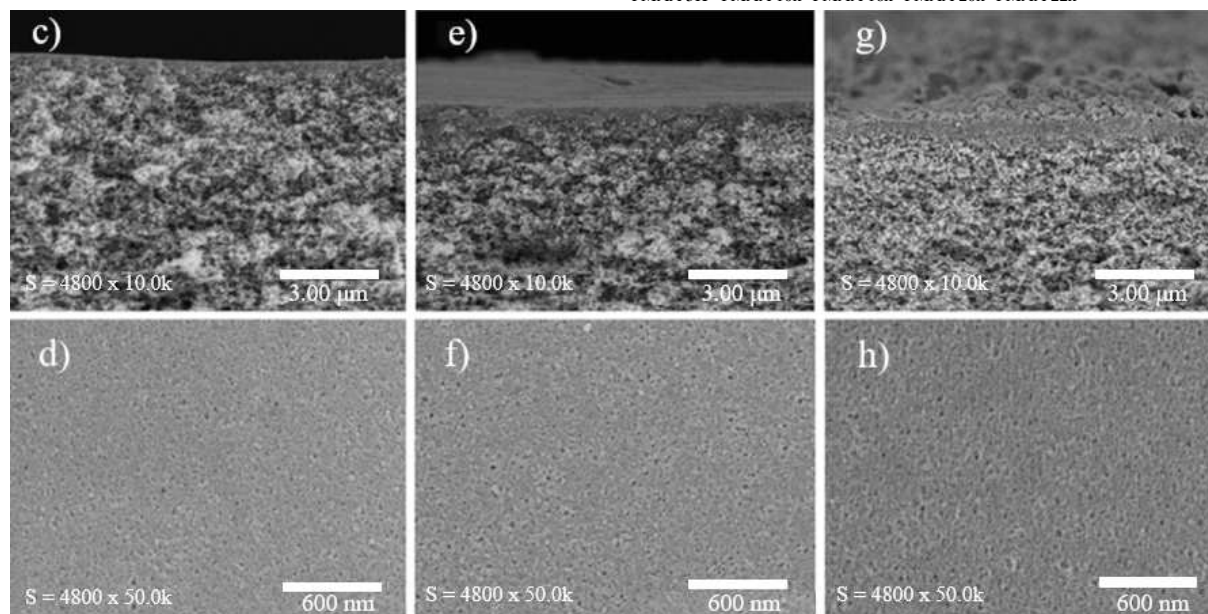
324 with  $J$  = transmembrane flux;  $N$  = pores number;  $dP$  = pressure gradient across the membrane;  $r$  = average pore  
325 radius;  $L$  = membrane thickness;  $\eta$  = fluid viscosity.

326 A 15 min deposition time was selected for the rest of the work, which is a good compromise between enough  
327 PDA functionalisation for the subsequent PMAA grafting and moderate flux decrease.

328



329



330

330 Figure 4 –a) Evolution of the flux ( $J$ ) after PDA deposition and after PMAA grafting as normalized by the flux  
 331 of the virgin membrane ( $J_0$ ), as a function of PMAA molecular weight, b) Water contact angle on virgin PES  
 332 membrane (MEM), PDA modified membrane (MEM PDA) and PMAA grafted membrane (MEM PMAA), c-h)  
 333 SEM images of cross sections (c, e, g) and top surfaces (d, f, h) of virgin PES membrane (c, d), 15 min PDA  
 334 coated PES membrane (e, f), and PMAA<sub>22k</sub> grafted membrane (g, h).

335

336 The functionalisation was indirectly characterized by the flux measurement (Figure 4a). A flux decrease  
 337 is observed after each functionalisation step from virgin PES membrane to PDA-modified membrane to PMAA-  
 338 grafted membrane. However, the decrease does not appear to be correlated with the molecular weight of the  
 339 grafted PMAA and ranges from 10 to 60% for the same PDA deposition time (15 min).

340 An increase of the surface hydrophilicity was also observed after each step, illustrated by the decrease  
 341 of the water contact angle (Figure 4b). If the trend is clear and constant, the water contact angle seems to be  
 342 sample dependent, with a dependence more relying on the varying surface roughness rather than the results of  
 343 the PMAA molecular weight for instance. Switching the water pH of the droplets from 7 to 3 did not provide a  
 344 clear tendency. It is assumed that it is the result of two antagonist effect: an acidic pH below the PMAA pKa will

345 result in the pore opening due to the polymer contraction. However, PMAA also became less hydrophilic at this  
346 pH, as did the membrane surface.

347 Each step of membrane modification has been characterized by SEM (Figure 4c-h). Although the top  
348 surface images do not show any real difference after functionalization steps, a thin layer of PDA and PMAA is  
349 well observed in the cross-section images. The EDX mapping (Figure SI-8) shows that PMAA is uniformly  
350 grafted with visible enrichment of carbon on the surface. The membrane bulk porosity was estimated from 1-  
351 butanol gravimetric analysis and a stable value around 77% is found for all membranes (porosity<sub>MEM</sub> = 77.5%;  
352 porosity<sub>MEM PDA 15 min</sub> = 77.7%; porosity<sub>MEM PMAA\_10k</sub> = 77.2%). Since only a surface modification is performed  
353 on an asymmetric PES membrane, the overall porosity is in return not affected. On the contrary, the time of PDA  
354 deposition is found to change surface porosity, as measured by SEM image treatment (porosity<sub>MEM</sub> = 7.8%;  
355 porosity<sub>MEM PDA 15 min</sub> = 3.4%; porosity<sub>MEM PDA 1 h</sub> = 3.5%; porosity<sub>MEM PDA 18 h</sub> = 1.5%). Similar trend is  
356 observed with PMAA grafting, which reduces surface porosity (porosity<sub>MEM PMAA\_22k (with PDA=15 min)</sub> = 2.3%), in  
357 agreement with a polymer coating/grafting.

358 Gravimetric analysis was carried out to estimate the weight of polymer deposited at the membrane  
359 surface after PDA coating and PMAA grafting (Table SI-3). As expected, a correlation between the PDA  
360 deposition time and the PDA quantity deposited is observed. Because PMAA is grafted onto the PDA layer, a  
361 direct link is observed between the quantity of PDA deposited and the yield of PMAA grafting. Interestingly, for  
362 the same PMAA grafting time, the grafted PMAA was 2.4 times higher when the deposited PDA was higher.  
363 Here it is suspected that 18h PDA coating has increased surface roughness and thus the specific PDA surface  
364 available for PMAA grafting. Young moduli (tensile test) were measured to see if the PMAA grafting would  
365 have an impact, but it appears that the deposition is too thin to make any significant difference (Table SI-4).

366 The surface composition was characterized by XPS analysis (Figure SI-9-19). However, unless a  
367 sufficient PDA layer is deposited (18h), the elemental compositions (C, N, O and S) of the PDA coated  
368 membranes remain similar to the PES commercial membrane. This is a further proof that the PDA deposition  
369 time chosen (15 minutes) allows a very thin layer to be deposited, sufficient to be able to functionalize without  
370 drastically changing the chemical nature of the interface. The XPS data (Table SI-5) shows that the carbon and  
371 nitrogen concentrations in PMAA grafted membranes are similar than in the commercial membrane, but the  
372 oxygen concentration rises with the polymer grafting, which is in line with the theory. It also appears that the  
373 sulfur concentration decreases for all the grafted samples, proving that deposition on the PES membrane is  
374 taking place.

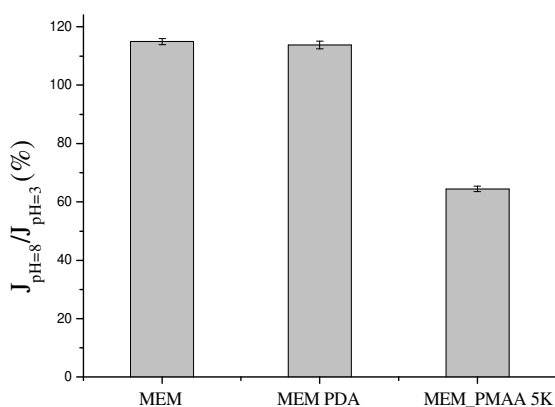
375 A measurement of the streaming potential was performed (Figure SI-7). A significantly different  
376 evolution of the calculated negative zeta potential is observed, attesting to the difference in surface chemistry.  
377 However, a similar isoelectric point (IEP) at pH 3-3.5 for the three samples, in agreement with reported PES  
378 IEP[46], suggests that only a partial coverage of the membrane surface occurs.

379

380 3.3 pH-induced self-oscillating flux

381

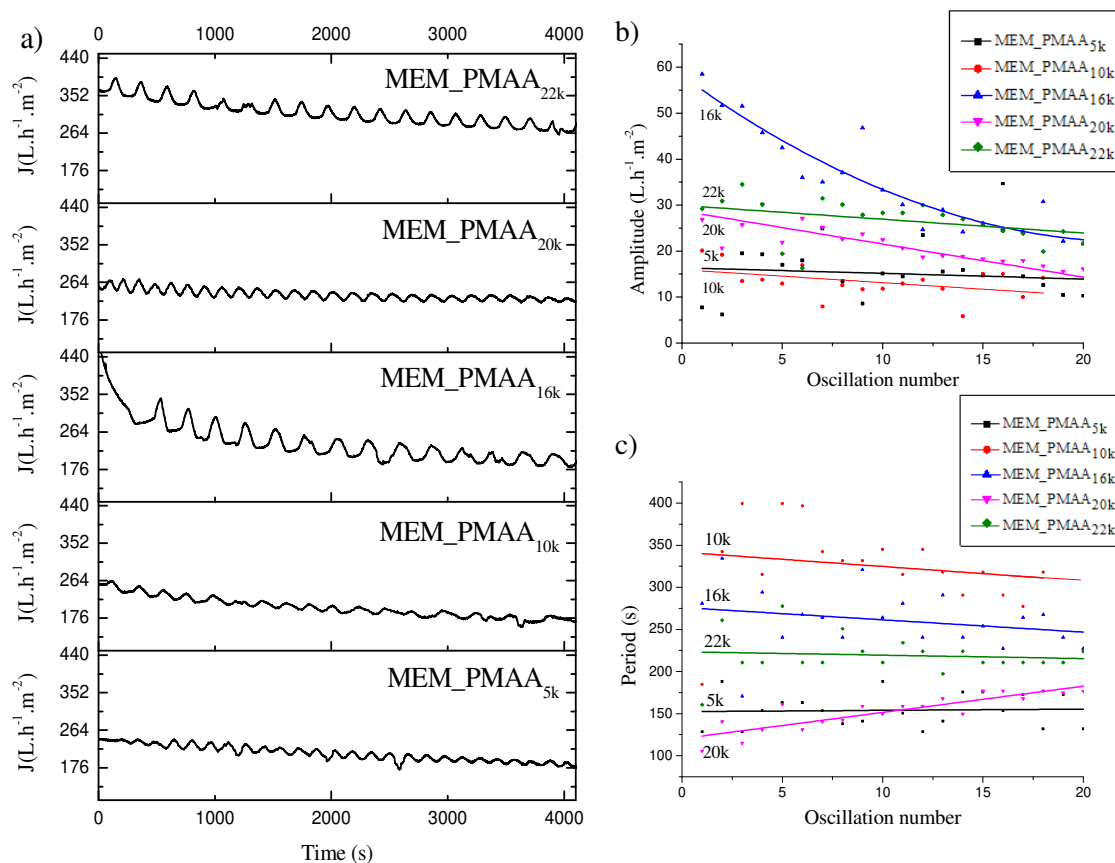
382 In order to yield a self-oscillating behavior, a pH-sensitive polymer membrane is mounted into a dead-  
 383 end filtration cell and synchronized with a pH oscillator (Figure SI-26). PMAA is a weak polyelectrolyte with a  
 384 quick conformation change as a function of pH. A globular conformation is observed for low degrees of  
 385 ionization, and the chains are collapsed due to the "hydrophobic" interactions with the methyl groups. The  
 386 membrane pores are then in an "open" state. The polymer chains expand abruptly above a pH threshold ( $pK_a =$   
 387 4.8) to release the electrostatic energy associated with deprotonation. The membrane pores are "closed" at this  
 388 point. The BSF pH oscillator can generate pH cycles ranging from 3.5 to 6.5 (Figure SI-22). The BSF oscillator  
 389 and the pH-sensitive membrane must be synchronized in order for the membrane pores to vary cyclically and to  
 390 thus observe a periodic variation of the transmembrane flux. The first step is to check the "unresponsiveness" of  
 391 the virgin PES membrane to pH in terms of water permeability. Thus, the virgin PES membrane was subjected to  
 392 sequential pH variations (3 and 7) (Figure SI-20). Ignoring the effect of the depressurization of the filtration cell  
 393 during the change of solutions, no significant change in flux was observed in relation to the pH. One can note a  
 394 natural tendency of transmembrane flux decrease over time despite the conditioning performed (see experimental  
 395 part for more details).



396  
 397 Figure 5 – Water flux ratio at pH 8 and 3 of the commercial PES membrane (MEM), the membrane coated with  
 398 PDA for 15 min (MEM\_PDA), and the membrane grafted with PMAA<sub>5k</sub> (MEM\_PMAA<sub>5k</sub>) at  $\Delta P = 1$  bar.

399 The pure water flux of the virgin PES membrane, the PDA coated membrane, and the PMAA grafted  
 400 membrane were then measured at pH values above and below the PMAA  $pK_a$  to assess its effect (Figure 5).  
 401 Whereas a slight increase in flux at basic pH is observed for commercial and PDA covered membranes, a clear  
 402 flux decreases of 40% at pH=8 is measured when PMAA is grafted onto the membrane. Indeed, above PMAA  
 403  $pK_a$  value, the polymer is in an expanded conformation which obstructs the pores and reduces their size. Since  
 404 the dependence is inversed compared to the PDA coated membrane, it can be deduced that PMAA membrane is  
 405 pH-sensitive and that a modulation of the pH results in a proportionate change in the water permeability. It  
 406 should be noted that the tolerance of the membrane towards acidic and alkaline operating conditions was  
 407 checked to avoid any misinterpretation. The water flux at  $\Delta P = 1$  bar of the virgin PES membrane and the  
 408 PMAA grafted membrane was measured at pH 3 and 10 for 15 days without showing any significant change  
 409 ( $J_{PES\ MEM, pH3} = 278 \pm 51$  L.h<sup>-1</sup>.m<sup>-2</sup>;  $J_{PES\ MEM, pH10} = 181 \pm 24$  L.h<sup>-1</sup>.m<sup>-2</sup>;  $J_{PMAA\ MEM, pH3} = 125 \pm 3$  L.h<sup>-1</sup>.m<sup>-2</sup>;  $J_{PMAA\ MEM, pH10} = 129 \pm 5$  L.h<sup>-1</sup>.m<sup>-2</sup>).

411 As explained before, autonomous cyclic pH change will be carried out thanks to the BSF chemical  
 412 oscillator setup in the filtration cell. BSF is an oscillating network of chemical reactions, which can be  
 413 summarized by a set of 7 reactions [39] (Table SI-6). The cyclic predominance of certain reactions in the BSF  
 414 oscillator leads to a modulation of the pH within a domain of residence time in the filtration cell. The residence  
 415 time domain to observe the pH oscillations was previously estimated from the construction of a bifurcation  
 416 diagram (Figure SI-21) [39] and a  $k_0$  value of  $10^{-3} \text{ s}^{-1}$  was targeted in this work,  $k_0$  being the inverse of the  
 417 residence time in the filtration cell. The pH oscillations produced from a BSF oscillator for a  $k_0$  of  $10^{-3} \text{ s}^{-1}$  have  
 418 an average period of about 390 s after stabilization with a pH varying cyclically and continuously between 3 and  
 419 6.5 (Figure SI-22). PMAA pKa being around 4.8, then the pH oscillations will enable change of conformation of  
 420 PMAA chains grafted on the membranes. Because of the inability to directly follow the pH change in a  
 421 pressurized filtration cell, a colored indicator was used to visually track the pH oscillation. The BSF reaction  
 422 alone was filmed and monitored by a pH-meter to see if the colored indicator is a reliable tracking system



423 (Figure SI-23). It appears that the visual color change and the pH change match perfectly.

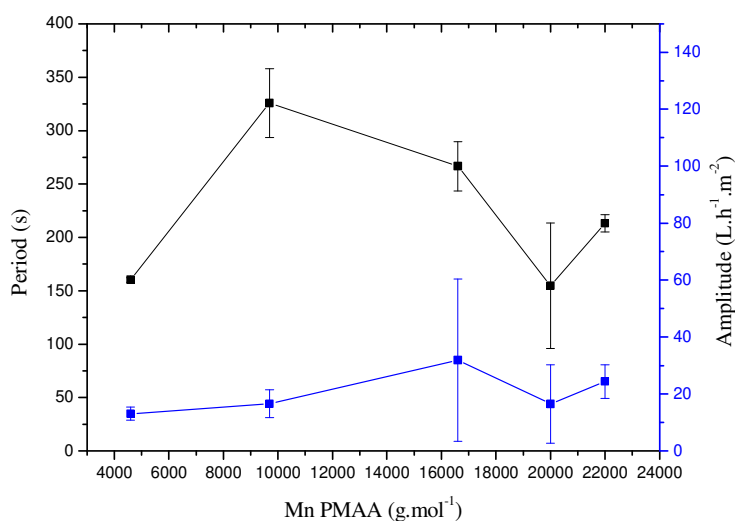
424

425 Figure 6 – a) Self-oscillating flux of functionalized membranes synchronized with a BSF oscillator with the  
 426 following conditions:  $[\text{KBrO}_3]_0 = 75 \text{ mM}$ ,  $[\text{Na}_2\text{SO}_3]_0 = 70 \text{ mM}$ ,  $[\text{K}_4\text{Fe}(\text{CN})_6]_0 = 15 \text{ mM}$ ,  $[\text{H}_2\text{SO}_4] = 7.5 \text{ mM}$  for T



427 = 30 °C and  $k_0 = 10^{-3} \text{ s}^{-1}$ ; b) Evolution of oscillation amplitude for each PMAA molecular weight; c) Evolution  
428 of oscillation period for each PMAA molecular weight. b-c) Fitting curves are shown only as a guide for the eye

429 When the BSF pH oscillator is set up in the filtration cell with PMAA-functionalised PES membranes,  
430 flux oscillations are observed as shown in Figure 6a. It appears that the molecular weight of PMAA greatly  
431 affects the flux oscillations, as much in amplitude than in period. Also, the BSF oscillator seems to be able to  
432 have a great stability under filtration conditions as self-oscillating flux could still be recorded after 35 cycles of  
433 pH (Figure SI-27). Figure 6b shows that there is a more or less pronounced decrease of the oscillation amplitude  
434 in time, with a variable intensity depending on the PMAA molecular weights. The PMAA chains remain  
435 hydrophilic all the time including below the pKa of the PMAA. However, as reported in literature, the grafted  
436 polymer onto the membrane surface may not be fully accessible to the bulk solution and some charges can  
437 remain avoiding a complete polymer collapsing over the cycles [47]. It can be noted that the greatest decrease in  
438 amplitude was observed with MEM\_PMAA16k. The oscillation periods represented in Figure 6c remain  
439 relatively stable over time, except for MEM\_PMAA20k, for which a slight increase is observed over time. As  
440 the oscillation period depends on the oscillator mechanism, it is complex to analyse the evolutions. However, it  
441 appears that all the periods are shorter than for the BSF oscillator alone, which shows that the membrane  
442 participates in the oscillating system. The molecular weight of the grafted PMAA appears to modulate both the  
443 period and the amplitude, as summarized in Figure 7.

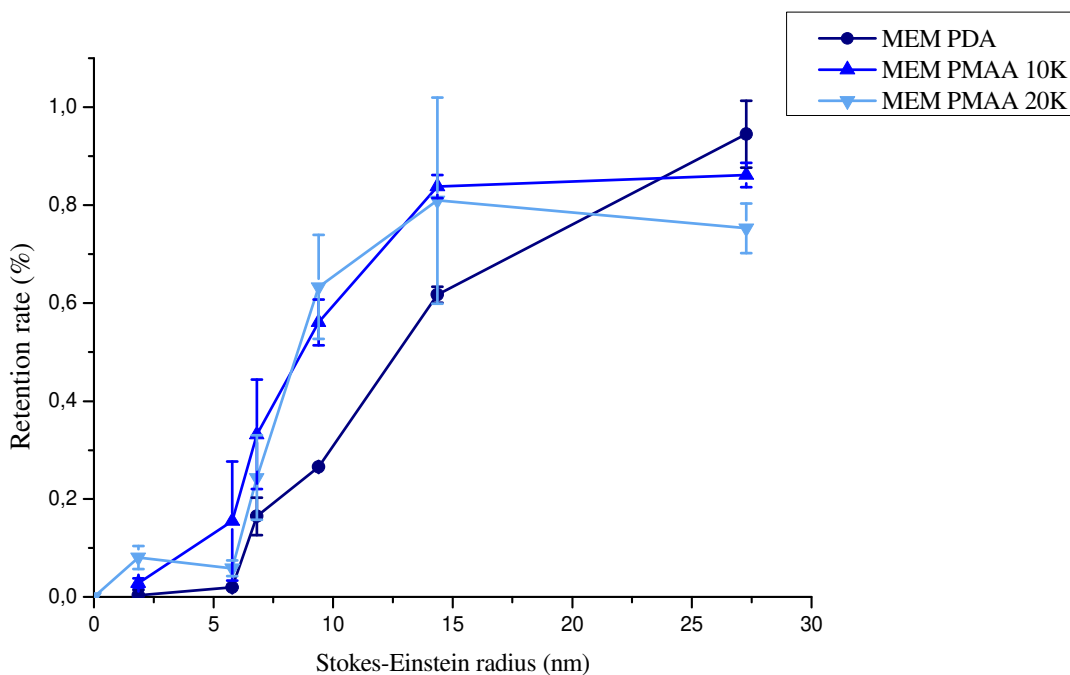


444

445 Figure 7 - Average amplitude and period of water flux oscillations for each PMAA molecular weight

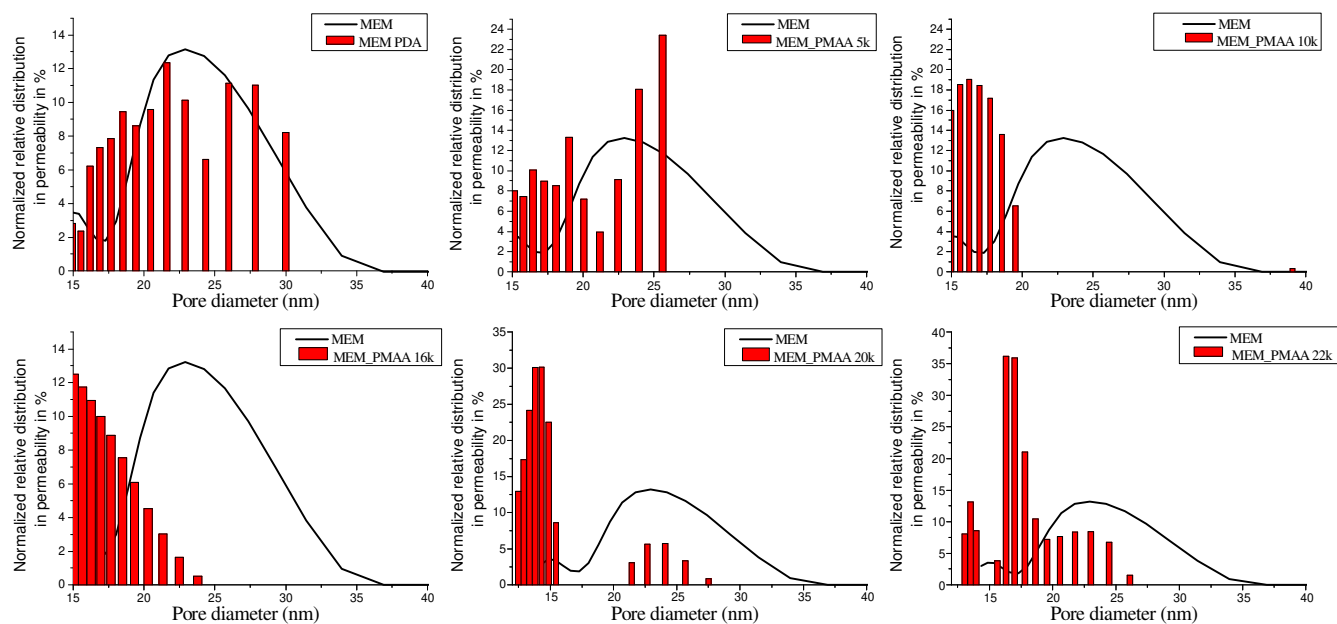
446 When the two parameters are compared in Figure 7, it appears that both values increase with the  
447 molecular weight of PMAA, then decrease for PMAA<sub>20k</sub>, before increasing again at PMAA<sub>22k</sub>. A hypothesis is  
448 that a steric exclusion occurs between Mn= 16 000 g.mol<sup>-1</sup> and 20 000 g.mol<sup>-1</sup>. A large amplitude can be  
449 observed when the PMAA is located inside the pores. When the PMAA chain length is increased, the flux  
450 change, corresponding to the compact and extended conformations of PMAA in the pores, is larger. However,  
451 above a threshold value of PMAA molecular weight, some steric hindrance can occur, preventing grafting inside  
452 the pores and thus leading to a decrease in the flux oscillation amplitude. A second increase above 20 000 g.mol<sup>-1</sup>  
453 is also observed which can be explain by an obstruction of the pores from the membrane surface. If the

454 hypothesis is correct, the pore size distribution for MEM\_PMAA<sub>10k</sub> and MEM\_PMAA<sub>20k</sub> would be significantly  
 455 different. Indeed, MEM\_PMAA<sub>10k</sub> would have a reduced pore size due to the presence of the polymer chains in  
 456 the pores, whereas grafting of MEM\_PMAA<sub>20k</sub> would have a lower pore size impact, being mostly located at the  
 457 membrane surface. The sieving curves, carried out with dextran of different molecular weights, are presented in  
 458 Figure 8.



459  
 460 Figure 8 – Sieving curve for ●) PDA coated membrane ▲) grafted membrane with PMAA =10 000 g.mol<sup>-1</sup> and  
 461 ▼) grafted membrane with PMAA =20 000 g.mol<sup>-1</sup>

462  
 463 The sieving curves were measured for two grafted PMAA molecular weights, PMAA<sub>10k</sub> and PMAA<sub>20k</sub>.  
 464 It should be first mentioned that a weak reproducibility was observed when repeating the sieving curve  
 465 measurements on different samples of the same membrane as illustrated by the large error bars obtained for the  
 466 virgin PES membrane (Figure SI-28) [48]. To try to overcome its impact, the sieving curves were made on the  
 467 same membrane for all the functionalisation steps (Figures 8). It appears that the PDA deposition has not clearly  
 468 shifted the sieving curve towards lower pore values as expected, which could be explained by a change in the  
 469 surface properties (hydrophilicity, roughness) counterbalancing the pore size decrease. Grafting of PMAA has  
 470 shifted the sieving curve to lower pore size, in agreement with the flux decrease observed previously. However,  
 471 considering the error bars, the sieving curves as measured with the two PMAA molecular weights did not  
 472 highlight a significant difference.



473

474 Figure 9 – Liquid-liquid porometry results for PES commercial membrane, PDA-coated membrane (15 min) and  
 475 membranes grafted with PMAA of different molecular weights.

476 Liquid-liquid porometry (Figure 9) shows that the commercial membrane has an average pore size of 22 nm and  
 477 a relatively large dispersity. The PDA deposition doesn't seem to affect significantly the pore size distribution.  
 478 However, when PMAA is grafted, the pore size distribution is shifted towards lower values in all cases, showing  
 479 that PMAA grafting is decreasing the pore size with a higher shift towards lower pore size with increasing  
 480 PMAA molecular weight, in agreement with the evolution of the water flux as previously discussed. However,  
 481 for the membranes grafted with PMAA  $\geq 20\ 000\ \text{g}\cdot\text{mol}^{-1}$ , a double distribution is observed with smaller pores as  
 482 in the case observed with PMAA lower than  $20\ \text{kg}\cdot\text{mol}^{-1}$ , but also with a remaining distribution of pore size from  
 483 the initial PDA membrane. A hypothesis is that a partial steric exclusion of PMAA from the membrane pores  
 484 appended leading to leave unfunctionalized a part of the initial pore size distribution. This is in agreement with  
 485 the break in water flux amplitude trend observed in Figure 7 at this PMAA molecular weight. We didn't succeed  
 486 in showing a clear shift of the pore size distribution from the sieving curves or from the porometry measurement  
 487 when comparing the results at pH below and above the PMAA pKa (data not shown). To understand that  
 488 observation, the expected pore size variation resulting from a pH below and above the PMAA pKa was  
 489 estimated from the measured water flux variations according to the Poiseuille law (equation 1) (Table SI-7).

490 A pore size change of maximum 2.5 to 6.5% (0.4 to 1.5 nm) is expected which explains the difficulty to directly  
 491 observe it following the pore size. It is however clearly visible in the flux measurement thanks to dependence of  
 492 the flux to the fourth power of the pore radius. We can therefore conclude that water flux self-oscillations have  
 493 been yielded without significantly alter the solute retention of membrane.

494 The BSF oscillator involves many ionic species whose concentration can vary with time depending on the  
 495 oscillatory regime. Given our use of a weak polyelectrolyte (PMAA), the impact of ionic strength on water  
 496 permeation results was checked. For this, the ionic strength of the oscillator ( $400\ \text{mmol}\cdot\text{L}^{-1}$ ) was reproduced by  
 497 adding NaCl ( $0.4\ \text{mol}\cdot\text{L}^{-1}$ ) to water. As shown in Figure SI-25, the transition from pure water to salted water was

498 not accompanied by a change in flux. In addition, a theoretical modeling of pH and ionic strength oscillations  
499 was performed (Figure SI-24) and only a weak ionic strength oscillation is observed between 414 and 420  
500 mmol.L<sup>-1</sup>. Thus, we can conclude that the ionic strength imposed by the pH oscillator does not impact the water  
501 permeation results. The flux oscillations are therefore only the results of the expansion-contraction cycles of the  
502 PMAA inside the membranes pores.

### 503 3. Conclusions

504

505 Self-oscillating polymer membranes showing continuous periodic flux evolution have been successfully  
506 prepared. The flux oscillations were obtained by coupling a pH-sensitive polymer membrane to a pH oscillator  
507 (BSF). For this, PMAA was synthesized with different molecular weights and grafted onto a commercial PES  
508 membrane via an intermediate layer of PDA. Each stage of polymer manufacturing and membrane  
509 functionalisation has been precisely characterized. Secondly, the pH oscillator was stabilized in a filtration cell  
510 and brought into contact with the pH-sensitive membrane. The PMAA grafted onto the membrane responds  
511 almost instantaneously to changes in pH and oscillates between two chain conformations (extended and  
512 collapsed). Therefore, an autonomous and cyclic membrane pore size change was observed leading to the self-  
513 oscillation of the membrane water flux. Interestingly, although water flux is periodically modulated, the  
514 corresponding pore size change due to the pH modulation is estimated to be less than 6%, which has  
515 immeasurable impact on the solute retention of membrane. In addition, the amplitude of the flux cycles can be  
516 modulated by the molecular weight of the PMAA grafted onto the membrane until a threshold value of 20 000  
517 g.mol<sup>-1</sup>, above which a polymer exclusion from the pores was observed. In perspective to this work, the effect of  
518 flux oscillations on the challenging fouling phenomenon will be explored since a perpetual change of the  
519 membrane surface properties combined with an adhesion of retained species hampered by flux oscillations could  
520 offer a more sustainable alternative to the usual mechanical and chemical membrane cleanings. Bringing self-  
521 oscillating behaviour to a polymer filtration membrane represents a further step towards the design of  
522 autonomous membranes.

523

### 524 Credit authorship contribution statement

525 **Johanne Pirkin-Benameur**: Conceptualization, Methodology, Data curation, Writing – original draft, Writing –  
526 review & editing. **Denis Bouyer**: Conceptualization, Methodology, Data curation. **Damien Quemener**:  
527 Conceptualization, supervision, acquisition of funds, data curation, writing - review & editing.

528

### 529 Declaration of Competing Interest

530 The authors declare no conflict of interest.

### 531 Acknowledgements

532 The authors thank the Institut Universitaire de France (IUF) and the Agence Nationale de la Recherche (ANR)  
533 through the OscMEM project (ANR-20-CE06-0013-01) for financial support. Valérie Flaud, Didier Cot, and  
534 Bertrand Rebiere are acknowledged for XPS, SEM, and EDX analysis.

## 535 References

536

- 537 [1] L. Persson, B.M.C. Almroth, C.D. Collins, S. Cornell, C.A. de Wit, M.L. Diamond, P. Fantke, M.  
538 Hassellöv, M. MacLeod, M.W. Ryberg, P.S. Jørgensen, P. Villarrubia-Gómez, Z. Wang, M.Z.  
539 Hauschild, Outside the Safe Operating Space of the Planetary Boundary for Novel Entities,  
540 Environmental Science & Technology. (2022) acs.est.1c04158.  
541 <https://doi.org/10.1021/ACS.EST.1C04158>.
- 542 [2] M. Wei, Y. Gao, X. Li, M.J. Serpe, Stimuli-responsive polymers and their applications, Polymer  
543 Chemistry. 8 (2016) 127–143. <https://doi.org/10.1039/C6PY01585A>.
- 544 [3] D. Roy, W.L. A. Brooks, B. S. Sumerlin, W.L.A. Brooks, B.S. Sumerlin, New directions in  
545 thermoresponsive polymers, Chemical Society Reviews. 42 (2013) 7214–7243.  
546 <https://doi.org/10.1039/C3CS35499G>.
- 547 [4] S. Dai, P. Ravi, K. Chiu Tam, K.C. Tam, {pH}-Responsive polymers : synthesis, properties and  
548 applications, Soft Matter. 4 (2008) 435–449. <https://doi.org/10.1039/B714741D>.
- 549 [5] D.A. Davis, A. Hamilton, J. Yang, L.D. Cremer, D. Van Gough, S.L. Potisek, M.T. Ong, P. V.  
550 Braun, T.J. Martínez, S.R. White, J.S. Moore, N.R. Sottos, Force-induced activation of covalent  
551 bonds in mechanoresponsive polymeric materials, Nature 2009 459:7243. 459 (2009) 68–72.  
552 <https://doi.org/10.1038/nature07970>.
- 553 [6] Y.L. Colson, M.W. Grinstaff, Y.L. Colson, M.W. Grinstaff, Biologically Responsive Polymeric  
554 Nanoparticles for Drug Delivery, Advanced Materials. 24 (2012) 3878–3886.  
555 <https://doi.org/10.1002/ADMA.201200420>.
- 556 [7] A. Fernández-Nieves, Engineering colloids with optical and geometrical anisotropies: de-  
557 coupling size monodispersity and particle properties, Soft Matter. 2 (2006) 105–108.  
558 <https://doi.org/10.1039/B512441G>.
- 559 [8] N.S. Terefe, O. Glagovskaia, K. De Silva, R. Stockmann, Application of stimuli responsive  
560 polymers for sustainable ion exchange chromatography, Food and Bioproducts Processing. 92  
561 (2014) 208–225. <https://doi.org/10.1016/J.FBP.2014.02.003>.
- 562 [9] G.W. De Groot, M.G. Santonicola, K. Sugihara, T. Zambelli, E. Reimhult, J. Vörös, G.J. Vancso,  
563 Switching transport through nanopores with pH-responsive polymer brushes for controlled  
564 ion permeability, ACS Applied Materials and Interfaces. 5 (2013) 1400–1407.  
565 [https://doi.org/10.1021/AM302820Y/SUPPL\\_FILE/AM302820Y\\_SI\\_001.PDF](https://doi.org/10.1021/AM302820Y/SUPPL_FILE/AM302820Y_SI_001.PDF).
- 566 [10] X. Gao, W. Yang, P. Pang, S. Liao, Q. Cai, K. Zeng, C.A. Grimes, A wireless magnetoelastic  
567 biosensor for rapid detection of glucose concentrations in urine samples, Sensors and  
568 Actuators B: Chemical. 128 (2007) 161–167. <https://doi.org/10.1016/J.SNB.2007.05.045>.
- 569 [11] D. Schmaljohann, Thermo- and pH-responsive polymers in drug delivery, Adv Drug Deliv Rev.  
570 58 (2006) 1655–1670. <https://doi.org/10.1016/J.ADDR.2006.09.020>.

- 571 [12] X. Yang, L. Chen, B. Huang, F. Bai, X. Yang, Synthesis of pH-sensitive hollow polymer  
572 microspheres and their application as drug carriers, *Polymer (Guildf)*. 50 (2009) 3556–3563.  
573 <https://doi.org/10.1016/J.POLYMER.2009.06.027>.
- 574 [13] P. Zarrintaj, M. Jouyandeh, M.R. Ganjali, B.S. Hadavand, M. Mozafari, S.S. Sheiko, M.  
575 Vatankhah-Varnoosfaderani, T.J. Gutiérrez, M.R. Saeb, Thermo-sensitive polymers in  
576 medicine: A review, *European Polymer Journal*. 117 (2019) 402–423.  
577 <https://doi.org/10.1016/J.EURPOLYMJ.2019.05.024>.
- 578 [14] J.B. Qu, L.Y. Chu, M. Yang, R. Xie, L. Hu, W.M. Chen, A pH-Responsive Gating Membrane  
579 System with Pumping Effects for Improved Controlled Release, *Advanced Functional*  
580 *Materials*. 16 (2006) 1865–1872. <https://doi.org/10.1002/ADFM.200500897>.
- 581 [15] G. Yi, X. Fan, X. Quan, H. Zhang, S. Chen, H. Yu, A pH-responsive PAA-grafted-CNT intercalated  
582 RGO membrane with steady separation efficiency for charged contaminants over a wide pH  
583 range, *Separation and Purification Technology*. 215 (2019) 422–429.  
584 <https://doi.org/10.1016/J.SEPPUR.2019.01.028>.
- 585 [16] Z. Chen, M.H.-Y. Chan, V.W.-W. Yam, Stimuli-Responsive Two-Dimensional Supramolecular  
586 Polymers Based on Trinuclear Platinum(II) Scaffolds: Reversible Modulation of  
587 Photoluminescence, Cavity Size, and Water Permeability., *J Am Chem Soc.* (2020).  
588 <https://doi.org/10.1021/jacs.0c07969>.
- 589 [17] Q. Ye, R. Wang, C. Chen, B. Chen, X. Zhu, High-Flux pH-Responsive Ultrafiltration Membrane  
590 for Efficient Nanoparticle Fractionation., *ACS Applied Materials & Interfaces*. (2021).  
591 <https://doi.org/10.1021/acsami.1c16673>.
- 592 [18] Z. Ma, G. Shu, X. Lu, Preparation of an antifouling and easy cleaning membrane based on  
593 amphiphobic fluorine island structure and chemical cleaning responsiveness, *Journal of*  
594 *Membrane Science*. (2020). <https://doi.org/10.1016/j.memsci.2020.118403>.
- 595 [19] J. Qiao, L. Liu, J. Shen, L. Qi, Enzyme immobilization on a pH-responsive porous polymer  
596 membrane for enzymatic kinetics study, *Chinese Chemical Letters*. 32 (2021) 3195–3198.  
597 <https://doi.org/10.1016/J.CCLET.2021.03.021>.
- 598 [20] K. Aissou, H. Bouzit, F. Krusch, J.P. Méricq, D. Cot, N. Masquelez, S. Roualdes, D. Quémener,  
599 Asymmetric Solvent-Annealed Triblock Terpolymer Thick Films Topped by a Hexagonal  
600 Perforated Lamellar Nanostructure, *Macromol Rapid Commun*. 43 (2022).  
601 <https://doi.org/10.1002/MARC.202100585>.
- 602 [21] T. Luo, S. Lin, R. Xie, X.J. Ju, Z. Liu, W. Wang, C.L. Mou, C. Zhao, Q. Chen, L.Y. Chu, pH-  
603 responsive poly(ether sulfone) composite membranes blended with amphiphilic polystyrene-  
604 block-poly(acrylic acid) copolymers, *Journal of Membrane Science*. 450 (2014) 162–173.  
605 <https://doi.org/10.1016/J.MEMSCI.2013.09.002>.
- 606 [22] H. Salehi, A. Shakeri, H. Mahdavi, R.G.H. Lammertink, Improved performance of thin-film  
607 composite forward osmosis membrane with click modified polysulfone substrate,  
608 *Desalination*. (2020). <https://doi.org/10.1016/j.desal.2020.114731>.
- 609 [23] M.G. Kochameshki, M. Mahmoudian, A. Marjani, K. Farhadi, M. Enayati, H.S. Mollayousefi,  
610 Graphene oxide grafted poly(acrylic acid) synthesized via surface initiated RAFT as a pH-  
611 responsive additive for mixed matrix membrane, *Journal of Applied Polymer Science*. (2019).  
612 <https://doi.org/10.1002/app.47213>.

- 613 [24] X. Deng, J.L. Livingston, N.J. Spear, G.K. Jennings, PH-Responsive Copolymer Films Prepared by  
614 Surface-Initiated Polymerization and Simple Modification., *Langmuir*. (2020).  
615 <https://doi.org/10.1021/acs.langmuir.9b03026>.
- 616 [25] A. Walther, A. Walther, Viewpoint: From Responsive to Adaptive and Interactive Materials  
617 and Materials Systems: A Roadmap, *Advanced Materials*. 32 (2020) 1905111.  
618 <https://doi.org/10.1002/adma.201905111>.
- 619 [26] T.S. Wong, S.H. Kang, S.K.Y. Tang, E.J. Smythe, B.D. Hatton, A. Grinthal, J. Aizenberg,  
620 Bioinspired self-repairing slippery surfaces with pressure-stable omniphobicity, *Nature* 2011  
621 477:7365. 477 (2011) 443–447. <https://doi.org/10.1038/nature10447>.
- 622 [27] G.R. Gossweiler, G.B. Hewage, G. Soriano, Q. Wang, G.W. Welshofer, X. Zhao, S.L. Craig,  
623 Mechanochemical activation of covalent bonds in polymers with full and repeatable  
624 macroscopic shape recovery, *ACS Macro Letters*. 3 (2014) 216–219.  
625 [https://doi.org/10.1021/MZ500031Q/SUPPL\\_FILE/MZ500031Q\\_SI\\_002.PDF](https://doi.org/10.1021/MZ500031Q/SUPPL_FILE/MZ500031Q_SI_002.PDF).
- 626 [28] X. Chen, M.A. Dam, K. Ono, A. Mal, H. Shen, S.R. Nutt, K. Sheran, F. Wudl, A thermally re-  
627 commendable cross-linked polymeric material, *Science* (1979). 295 (2002) 1698–1702.  
628 [https://doi.org/10.1126/SCIENCE.1065879/SUPPL\\_FILE/1065879S3\\_THUMB.GIF](https://doi.org/10.1126/SCIENCE.1065879/SUPPL_FILE/1065879S3_THUMB.GIF).
- 629 [29] S.R. White, J.S. Moore, N.R. Sottos, B.P. Krull, W.A. Santa Cruz, R.C.R. Gergely, Restoration of  
630 large damage volumes in polymers, *Science* (1979). 344 (2014) 620–623.  
631 [https://doi.org/10.1126/SCIENCE.1251135/SUPPL\\_FILE/WHITE-SM.PDF](https://doi.org/10.1126/SCIENCE.1251135/SUPPL_FILE/WHITE-SM.PDF).
- 632 [30] C.W. Park, S.K. Kang, H.L. Hernandez, J.A. Kaitz, D.S. Wie, J. Shin, O.P. Lee, N.R. Sottos, J.S.  
633 Moore, J.A. Rogers, S.R. White, Thermally triggered degradation of transient electronic  
634 devices, *Adv Mater*. 27 (2015) 3783–3788. <https://doi.org/10.1002/ADMA.201501180>.
- 635 [31] R. Yoshida, T. Takahashi, T. Yamaguchi, H. Ichijo, Self-Oscillating Gel, *Undefined*. 118 (1996)  
636 5134–5135. <https://doi.org/10.1021/JA9602511>.
- 637 [32] S. Maeda, Y. Hara, T. Sakai, R. Yoshida, S. Hashimoto, Self-Walking Gel, *Advanced Materials*.  
638 19 (2007) 3480–3484. <https://doi.org/10.1002/ADMA.200700625>.
- 639 [33] R. Yoshida, Y. Murase, Self-oscillating surface of gel for autonomous mass transport, *Colloids  
640 and Surfaces B: Biointerfaces*. 99 (2012) 60–66.  
641 <https://doi.org/10.1016/J.COLSURFB.2011.09.036>.
- 642 [34] D. Suzuki, T. Kobayashi, R. Yoshida, T. Hirai, Soft actuators of organized self-oscillating  
643 microgels, *Soft Matter*. 8 (2012) 11447–11449. <https://doi.org/10.1039/C2SM26477C>.
- 644 [35] T. Sakata, S. Nishitani, Y. Yasuoka, S. Himori, K. Homma, T. Masuda, A.M. Akimoto, K. Sawada,  
645 R. Yoshida, Self-oscillating Chemoelectrical Interface of Solution-gated Ion-sensitive Field-  
646 effect Transistor Based on Belousov–zhabotinsky Reaction, *Null*. (2021).  
647 <https://doi.org/10.21203/rs.3.rs-1110032/v1>.
- 648 [36] T. Yamamoto, R. Yoshida, Self-oscillation of polymer and photo-regulation by introducing  
649 photochromic site to induce LCST changes, *Reactive and Functional Polymers*. 73 (2013) 945–  
650 950. <https://doi.org/10.1016/J.REACTFUNCTPOLYM.2013.02.015>.
- 651 [37] K. Homma, Y. Ohta, K. Minami, G. Yoshikawa, K. Nagase, A.M. Akimoto, R. Yoshida,  
652 Autonomous Nanoscale Chemomechanical Oscillation on the Self-Oscillating Polymer Brush

- 653 Surface by Precise Control of Graft Density., *Langmuir*. (2021).  
654 <https://doi.org/10.1021/acs.langmuir.1c00459>.
- 655 [38] T. Geher-Herczegh, Z. Wang, T. Masuda, R. Yoshida, N. Vasudevan, Y. Hayashi, Delayed  
656 Mechanical Response to Chemical Kinetics in Self-Oscillating Hydrogels Driven by the  
657 Belousov-Zhabotinsky Reaction., *Macromolecules*. (2021).  
658 <https://doi.org/10.1021/acs.macromol.1c00402>.
- 659 [39] M. Benoit, D. Bouyer, P. Sizat, A. Ayrat, D. Cot, B. Rebiere, D. Fournier, J. Lyskawa, P. Woisel,  
660 C. Antonelli, D. Quemener, Self-Oscillating Membranes with Polymer Interface Synchronized  
661 with Chemical Oscillator to Reproduce Lifelike Pulsatile Flow, *Chemistry of Materials*. 33  
662 (2021) 998–1005. <https://doi.org/10.1021/acs.chemmater.0c04009>.
- 663 [40] M.R. Whittaker, Y.K. Goh, H. Gemici, T.M. Legge, S. Perrier, M.J. Monteiro, Synthesis of  
664 Monocyclic and Linear Polystyrene Using the Reversible Coupling/Cleavage of Thiol/Disulfide  
665 Groups, *Macromolecules*. 39 (2006) 9028–9034. <https://doi.org/10.1021/MA061070E>.
- 666 [41] E. Cazares-Cortes, B.C. Baker, K. Nishimori, M. Ouchi, F. Tournilhac, Polymethacrylic Acid  
667 Shows Thermoresponsivity in an Organic Solvent, *Macromolecules*. 52 (2019) 5995–6004.  
668 <https://doi.org/10.1021/acs.macromol.9b00412>.
- 669 [42] I. Lacík, M. Stach, P. Kasák, V. Semak, L. Uhelská, A. Chovancová, G. Reinhold, P. Kilz, G.  
670 Delaittre, B. Charleux, I. Chaduc, F. D’Agosto, M. Lansalot, M. Gaborieau, P. Castignolles, R.G.  
671 Gilbert, Z. Szablan, C. Barner-Kowollik, P. Hesse, M. Buback, SEC Analysis of Poly(Acrylic Acid)  
672 and Poly(Methacrylic Acid), *Macromolecular Chemistry and Physics*. 216 (2015) 23–37.  
673 <https://doi.org/10.1002/MACP.201400339>.
- 674 [43] H. Lee, S.M. Dellatore, W.M. Miller, P.B. Messersmith, Mussel-inspired surface chemistry for  
675 multifunctional coatings, *Science* (1979). 318 (2007) 426–430.  
676 [https://doi.org/10.1126/SCIENCE.1147241/SUPPL\\_FILE/LEE.SOM.PDF](https://doi.org/10.1126/SCIENCE.1147241/SUPPL_FILE/LEE.SOM.PDF).
- 677 [44] M. Gu, J. Zhang, X. Wang, H. Tao, L. Ge, Formation of poly(vinylidene fluoride) (PVDF)  
678 membranes via thermally induced phase separation, *Desalination*. 192 (2006) 160–167.  
679 <https://doi.org/10.1016/J.DESAL.2005.10.015>.
- 680 [45] Y. Chen, X. Feng, Y. Zhao, X. Zhao, X. Zhang, Mussel-Inspired Polydopamine Coating Enhances  
681 the Intracutaneous Drug Delivery from Nanostructured Lipid Carriers Dependently on a  
682 Follicular Pathway, *Molecular Pharmaceutics*. 17 (2020) 1215–1225.  
683 [https://doi.org/10.1021/ACS.MOLPHARMACEUT.9B01240/SUPPL\\_FILE/MP9B01240\\_SI\\_001.PDF](https://doi.org/10.1021/ACS.MOLPHARMACEUT.9B01240/SUPPL_FILE/MP9B01240_SI_001.PDF).
- 684 DF.
- 685 [46] H. Sadegh, R. Sahay, S. Soni, Protein–polymer interaction: Transfer loading at interfacial  
686 region of PES-based membrane and BSA, *Undefined*. 136 (2019).  
687 <https://doi.org/10.1002/APP.47931>.
- 688 [47] F. Schacher, M. Ulbricht, A.H.E. Müller, Self-Supporting, Double Stimuli-Responsive Porous  
689 Membranes From Polystyrene-block-poly(N,N-dimethylaminoethyl methacrylate) Diblock  
690 Copolymers, *Advanced Functional Materials*. 19 (2009) 1040–1045.
- 691 [48] R.I. Peinador, J.I. Calvo, K. ToVinh, V. Thom, P. Prádanos, A. Hernández, Liquid-liquid  
692 displacement porosimetry for the characterization of virus retentive membranes,  
693 *Journal of Membrane Science*. 372 (2011) 366–372.  
694 <https://doi.org/10.1016/J.MEMSCI.2011.02.022>.



# Graphical Abstract

